Extracting irreversible dephasing rates from electric dipole echoes in Rydberg Stark wave packets

S. Yoshida,[1] C. O. Reinhold,[2,3] J. Burgdörfer,[1,3] W. Zhao,[4] J. J. Mestayer,[4] J. C. Lancaster,[4] and F. B. Dunning[4]
[1]*Institute for Theoretical Physics, Vienna University of Technology, Vienna, Austria*
[2]*Physics Division, Oak Ridge National Laboratory, Oak Ridge, Tennessee 37831-6372, USA*
[3]*Department of Physics, University of Tennessee, Knoxville, Tennessee 37996, USA*
[4]*Department of Physics and Astronomy and the Rice Quantum Institute, Rice University, Houston, Texas 77005-1892, USA*
(Received 7 May 2008; published 17 December 2008)

The precession of an electric dipole moment in an external electric field can be reversed by reversing the field direction. This time-reversal operation allows study of coherence in the time evolution of Rydberg Stark wave packets by measuring the resulting echoes. Different sources of reversible dephasing and irreversible dephasing, i.e., decoherence, are discussed in detail. Stochastic interactions with the environment are simulated in a controlled manner by using artificially synthesized noise. The rate of irreversible dephasing is determined from the reduction of the echo amplitude under multiple field reversals.

DOI: 10.1103/PhysRevA.78.063414 PACS number(s): 32.80.Rm, 32.80.Qk, 76.60.Lz

I. INTRODUCTION

Many microscopic descriptions of decoherence and the approach toward equilibrium in nonequilibrium statistical physics rely on the concept of "open quantum systems" or their classical analog, open classical systems. Accordingly, only a subsystem with a small number of degrees of freedom is treated within the framework of Hamiltonian dynamics. Its interactions with the large number of neglected degrees of freedom, the so-called environment or noise, are too complex to be included microscopically and only their statistical properties, such as the average coupling strength and the fluctuation spectrum, are considered. The time evolution of the open system and of expectation values of system observables are determined as ensemble expectation values over different realizations of the environmental interactions. Two classes of environmental fluctuations are to be distinguished when the approach toward equilibrium or relaxation ("the arrow of time") is considered: spatial fluctuations (or inhomogeneities) and temporal fluctuations (or stochastic variations) of the coupling to the environment. The key to this distinction lies in their different properties under time reversal. For coupling to an environment exhibiting spatial fluctuations, the dynamics of each member of the ensemble is reversible. The phase fluctuations in the time evolution which lead to dephasing and decay of nonequilibrium expectation values can be reversed, allowing rephasing. In contrast, temporal stochastic fluctuations are not invariant under time reversal. They give rise to irreversible dephasing often referred to as decoherence and render the dynamics intrinsically irreversible. The rate of decoherence is of interest for quantum-information processing [1] where information is stored as a coherent superposition, or for coherent control of quantum systems [2] where a desired coherent superposition can be maintained only until decoherence sets in. The decoherence rate (or the dephasing rate) can be used to probe the coupling strength between an isolated system and its environment [3]. Distinguishing reversible from irreversible dephasing, which is a prerequisite for the determination of the decoherence rate, remains a challenge. For example, when the damping of "quantum beats," i.e., temporal oscillations due to the coherent superposition of nondegenerate states, is observed, both static and stochastic couplings are involved. If now an operation mimicking time reversal can be devised, that part of the dephasing resulting from static couplings can be reversed, leading to an increase in the amplitude of the quantum beats. Such a forced revival of the quantum beats is termed an echo. Echoes have been seen in nuclear magnetic resonance (NMR) as rephasing of nuclear spin precession around an external magnetic field ("spin echo" [4]) and in quantum optics as realignment of polarization induced in matter interacting with coherent light ("photon echo" [5]). The reduction of the amplitude of the echoes provides a measure of the decoherence: echoes that recover fully the initial beat amplitude show that no significant decoherence has occurred whereas the lack of any echo points to complete decoherence.

The precession of the electric dipole moments of Rydberg atoms in external electric fields has recently been shown to display echoes [6–8]. If the wave packet comprises a coherent superposition of either redshifted or blueshifted Stark states, the atom forming the wave packet has a (quasi)permanent dipole that will precess about the externally applied static electric field. A reversal of the field direction reverses the dipole precession, allowing the generation of echoes. Such time reversal was first demonstrated using an ensemble of wave packets, each of which was a superposition of two Stark states [6]. Recently, echoes of the electric dipole have been observed for an ensemble where each wave packet is a superposition of many Stark states [8]. This system features many similarities with the dynamics of nuclear spins while providing an ideal testing ground for discriminating between reversible and irreversible dynamics. Its equation of motion closely mirrors the Bloch equation of NMR. Moreover, for the system observables, i.e., the evolution of the dipole moments, a close classical-quantum correspondence holds. Unlike NMR, however, the interaction with the "environment" can be microscopically accounted for since other internal atomic degrees of freedom provide a significant part of the environment of the "system," the precessing electric dipoles.

While the dynamics of the electric dipoles can be almost fully controlled by using external electric fields, their coupling to the "atomic environment" can also be, to a certain degree, controlled and manipulated. In very high Rydberg states ($n \gtrsim 350$) characteristic precession times are such that atomic dephasing and rephasing can be conveniently observed without recourse to short-pulse lasers. Thus, Rydberg Stark wave packets can be used to study the coherences which we can experimentally maintain, control, and probe. In this paper we analyze the dynamics of Rydberg atoms in a static electric field in detail and demonstrate both experimentally and theoretically how to extract information on the time reversibility of the dynamics.

The outline of the paper is as follows. In Sec. II, we review in detail the dynamics of a hydrogenic Rydberg atom in a static electric field. Similar to the dynamics of spins in NMR, the dynamics of the electric dipole moment averaged over an ensemble of quantum Stark wave packets is well represented by the classical dynamics. In Sec. III we discuss basic mechanisms for reversible and irreversible dephasing. The present echo technique is introduced in Sec. IV, where we describe how to observe echoes by reversing the direction of the dc field. Since such field reversal only approximates a time-reversal operation and does not affect the other degrees of freedom of the electronic wave packet, this system features an intrinsic source of "irreversible" dephasing or decoherence. The origin of the different sources of dephasing is discussed together with a method to quantify the dephasing rates. Irreversible and reversible dephasing can be identified and separately determined. Dephasing rates can be manipulated and controlled (Sec. V) by introduction of tailored "colored" noise. Experimental results for highly excited Rydberg wave packets ($n \sim 350$) are presented in Sec. VI, followed by concluding remarks in Sec. VII. Atomic units are used unless indicated otherwise.

II. DYNAMICS OF AN ATOM IN A STATIC ELECTRIC FIELD

We analyze in the following both the classical and quantum dynamics in Coulomb systems in order to highlight the close classical-quantum correspondence for observables calculated using quantum and classical perturbation theory. This correspondence plays a key role in extracting (quantum) reversible and irreversible dephasing from classical dynamics.

A. Classical dynamics

Consider first the classical evolution of a hydrogenic Rydberg atom in the absence of an external electric field. The electron follows an elliptic orbit specified by the Hamiltonian

$$H_{\mathrm{at}} = \frac{p^2}{2} - \frac{1}{r}, \tag{1}$$

where $\vec{r}=(x,y,z)$ and $\vec{p}=(p_x,p_y,p_z)$ are its coordinate and momentum, respectively. The eccentricity and orientation of the ellipse are determined by the angular momentum $\vec{L}=\vec{r}\times\vec{p}$ and the Runge-Lenz vector $\vec{A}=\vec{p}\times\vec{L}-(1/r)\vec{r}$ [9], both of which are constants of motion. When the atom is subject to a static electric field F directed along the z axis, the Hamiltonian becomes

$$H = H_{\mathrm{at}} + zF, \tag{2}$$

and the angular momentum and Runge-Lenz vectors precess about the z axis. In the following we analyze the evolution of the Kepler ellipse characterized by these vectors rather than following the temporal position of the electron $(\vec{r}(t),\vec{p}(t))$ along the ellipse. The two vectors $\vec{L}$ and $\vec{A}$ are coupled to each other through the perturbation zF and their magnitudes vary periodically in time [10,11]. To first order in F, this periodic variation can be removed by a transformation to the so-called pseudospins [10]

$$\vec{J}^{\pm} = \frac{1}{2}(\vec{L} \pm n\vec{A}) \tag{3}$$

where $n=1/\sqrt{2|H_{\mathrm{at}}|}$. Within the framework of the secular perturbation approach [12], H_{at}, J_z^+, and J_z^- change adiabatically and are considered to be constants of motion at each instant. The perpendicular components (along x and y) of the pseudospins precess about the field z axis after the fast motion on the time scale of the Kepler orbital motion has been "adiabatically eliminated." In order to describe this procedure, it is useful to define the zeroth-order expectation value of an observable O over an unperturbed Coulomb orbit,

$$\langle O\rangle_0 = \int d^3r\, d^3p\, O(\vec{r},\vec{p})\rho_{\mathrm{cl}}^0(\vec{r},\vec{p}) = \frac{1}{T_n}\oint dt' O(\vec{r}_0(t'),\vec{p}_0(t')), \tag{4}$$

given by the average over a phase space distribution $\rho_{\mathrm{cl}}^0(\vec{r},\vec{p})$ given by the ensemble of points belonging to an unperturbed Coulomb orbit. The expectation value is equivalent to a time average of the observable along the unperturbed Coulomb orbit $(\vec{r}_0(t),\vec{p}_0(t))$, over the Kepler orbital period $T_n=2\pi n^3$. The orbital-averaged value is the classical analog to the quantum matrix element of the same observable O in a quantum state with quantum numbers given by the classical actions. Within first-order secular perturbation theory, the pseudospin dynamics are described by the orbital-averaged equation of motion

$$\frac{d}{dt}\vec{J}^{\pm} \simeq \langle\{\vec{J}^{\pm},H\}\rangle_0 = \frac{1}{T_n}\oint \{\vec{J}^{\pm},H\}dt'. \tag{5}$$

This coarse graining (i.e., orbital averaging) smoothes out the fast oscillation in the Poisson bracket $\{\vec{J}^{\pm},H\}$ on a time scale of T_n. To simplify the notation in the remainder of this section the brackets will be dropped and all quantities will be taken to refer to orbital-time-averaged quantities. One consequence of coarse graining in Eq. (5) is that the fast orbital motion along the Kepler ellipse becomes an unobserved degree of freedom when we consider the system Hamiltonian $H=H(H_{\mathrm{at}},J_z^+,J_z^-)$ as a function of the orbital-averaged actions J_z^+,J_z^-. As a result of the reduction of the problem to the precessional motion of two pseudo-spins, part of the internal atomic motion takes on the role of an environmental degree of freedom, i.e., under suitable circumstances the atomic dy-

namics can become the source of dephasing and decoherence for the pseudospin dynamics. We will exploit this remarkable feature in the following.

The orbital-averaged ("secular") equation of motion for the pseudospins is

$$\frac{d}{dt}\vec{J}^{\pm} = \frac{\partial H}{\partial H_{\rm at}}\{\vec{J}^{\pm},H_{\rm at}\} + \frac{\partial H}{\partial J_z^+}\{\vec{J}^{\pm},J_z^+\} + \frac{\partial H}{\partial J_z^-}\{\vec{J}^{\pm},J_z^-\} = \omega_{\pm}\vec{J}_{\pm}\times\hat{z} \tag{6}$$

with $\omega_{\pm}=-\partial H/\partial J_z^{\pm}$. Here we have used the classical version of the commutation relations, the Poisson brackets

$$\{J_\alpha^{\pm},J_\beta^{\pm}\} = \varepsilon_{\alpha\beta\gamma}J_\gamma^{\pm}, \quad \{J_\alpha^{\pm},J_\beta^{\mp}\} = 0, \quad \{J_\alpha^{\pm},H_{\rm at}\} = 0, \tag{7}$$

where $\alpha,\beta,\gamma=x,y,z$, and $\varepsilon_{\alpha\beta\gamma}$ is the Levi-Cività symbol. The last commutation relation indicates that in the absence of an external field the pseudospins are conserved. The effective Hamiltonian used in Eq. (6) can be written to first order in F as

$$H = H_{\rm at} + \langle z\rangle_0 F \simeq H_{\rm at} + \frac{3n}{2}(J_z^- - J_z^+)F, \tag{8}$$

using the orbital period average

$$\langle z\rangle_0 = -\frac{3}{2}n^2A_z = \frac{3}{2}n(J_z^- - J_z^+), \tag{9}$$

taken over the unperturbed Kepler motion [Eq. (5)]. Consequently the pseudospin precession frequencies are determined as $\omega_{\pm}=-\partial H/\partial J_z^{\pm}=\pm(3/2)nF$. Equation (6) resembles the Bloch equation [13] for (nuclear) spin precession in a magnetic field in NMR [3] in the limit of vanishing transverse and longitudinal relaxation. In the present case, however, the dynamics are characterized by a pair of counterpropagating pseudospins, each having one effective degree of freedom, the azimuthal angle $\phi_{\pm}^J \equiv \arctan(J_y^{\pm}/J_x^{\pm}) = \omega_{\pm}t$. In first-order perturbation theory the two pseudospins are decoupled. They become coupled, however, upon inclusion of second-order corrections. To this order, the secular Hamiltonian becomes

$$\begin{aligned} H &= -\frac{1}{2n^2} + \frac{3}{2}nkF - \frac{1}{16}F^2n^4(17n^2 - 3k^2 - 9m^2 + 19) \\ &= -\frac{1}{2n^2} + \frac{3}{2}n(J_z^- - J_z^+)F - \frac{1}{16}F^2n^4 \\ &\quad\times\{17n^2 - 12[(J_z^+)^2 + (J_z^-)^2 + J_z^+J_z^-] + 19\}, \end{aligned} \tag{10}$$

where $J_z^{\pm}=(1/2)(m\mp k)$ and we have expressed the classical actions in terms of their corresponding "quantum" numbers

$$m = L_z, \quad k = -nA_z = J_z^- - J_z^+. \tag{11}$$

We exploit here the (almost) complete classical-quantum correspondence. Equation (11) holds identically in quantum mechanics except that (m,k) are integer values. Likewise, Eq. (10) is valid in second-order quantum perturbation theory as well. The only difference is the additional term, constant within each n manifold, $-(19/16)F^2n^4$, which results from the noncommutativity of complementary variables. This quantum correction is included in Eq. (10) for completeness.

With the secular Hamiltonian [Eq. (10)], the dynamics of the pseudospins are still approximated by the Bloch equation [Eq. (6)] but with modified precession frequencies,

$$\omega_{\pm}(F) = -\frac{\partial H}{\partial J_z^{\pm}} = \pm[\omega_k^{(1)}(F) - \omega_k^{(2)}(F)] - \omega_m^{(2)}(F) \tag{12}$$

with $\omega_k^{(1)}(F)=(3/2)nF$, $\omega_k^{(2)}(F)=(3/8)n^4kF^2$, and $\omega_m^{(2)}(F)=(9/8)n^4mF^2$. Inclusion of second-order terms yields a good approximation to the pseudospin dynamics even for relatively strong external fields. Elimination of the additional fast degree of freedom underlying Eqs. (8) and (10) introduces, via coarse graining, corrections to Eq. (8) which can cause decoherence even in the absence of any external stochastic perturbation. This decoherence process can be fully accounted for by solving the full classical equations of motion without orbital averaging. The dephasing (or relaxation) terms in the Bloch equations [Eq. (6)] originating from this source can thus be microscopically determined. Clearly, other sources of environmental noise also contribute to dephasing and must be treated differently.

B. Quantum dynamics

As expected from the correspondence principle, it is also possible to derive the Bloch equation [Eq. (6)] quantum mechanically [14]. We consider a Stark wave packet which is a superposition of pseudospin eigenstates

$$|\psi(t)\rangle = \sum_{n,j_+,j_-} c_{n,j_+,j_-}(t)|n,j_+,j_-\rangle, \tag{13}$$

where $|n,j_+,j_-\rangle$ is an eigenstate of the operators $H_{\rm at}$, $J_z^{\pm}$ with eigenvalues $-1/(2n^2)$, $j_{\pm}$. The pseudospin eigenstates are parabolic states $|n,j_+,j_-\rangle=|n,k,m\rangle$ where $k=j_--j_+$ and $m=j_++j_-$. The Runge-Lenz operator entering in the pseudospins [Eq. (3)] has to be antisymmetrized as $\vec{A}=(1/2)(\vec{p}\times\vec{L}-\vec{L}\times\vec{p})-\hat{r}$ so that the operator becomes Hermitian [15]. Expressed in terms of the density operator $\rho(t)$, the time evolution of the expectation values of the pseudospins is given by the Liouville–von Neumann equation

$$i\frac{d}{dt}\langle\vec{J}^{\pm}(t)\rangle_{n,j_+,j_-} = \langle n,j_+,j_-|[\vec{J}^{\pm},H]\rho(t)|n,j_+,j_-\rangle, \tag{14}$$

where $\langle\vec{J}^{+}\rangle_{n,j_+,j_-}=\langle n,j_+,j_-|\vec{J}^{+}\rho(t)|n,j_+,j_-\rangle$.

For weak fields, the eigenenergy of the total Hamiltonian H is given in first-order degenerate perturbation theory by

$$E_{n,j_+,j^-} = -\frac{1}{2n^2} + \frac{3}{2}n(j_- - j_+)F. \tag{15}$$

The dipole matrix $\langle n,j_+,j_-|z|n',j_+',j_-'\rangle$ is diagonal within a single n manifold but couples different n manifolds. The operator equivalence $z=(3/2)n(J_z^- - J_z^+)$ holds only within the Hilbert subspace of fixed n. In order to transform Eq. (14) to the Bloch equation, we introduce the ladder operators $\mathcal{J}_{\pm},\mathcal{J}_{\pm}^{\dagger}$ defined as

$$J_x^{\pm} = \frac{1}{2}(\mathcal{J}_{\pm}^{\dagger} + \mathcal{J}_{\pm}), \quad J_y^{\pm} = -\frac{i}{2}(\mathcal{J}_{\pm}^{\dagger} - \mathcal{J}_{\pm}), \tag{16}$$

which act as raising and lowering operators on the pseudospin states

$$\mathcal{J}_+^{\dagger}|n,j_+,j_-\rangle \propto |n,j_+ + 1,j_-\rangle,$$

$$\mathcal{J}_+|n,j_+,j_-\rangle \propto |n,j_+ - 1,j_-\rangle,$$

$$\mathcal{J}_-^{\dagger}|n,j_+,j_-\rangle \propto |n,j_+,j_- + 1\rangle,$$

$$\mathcal{J}_-|n,j_+,j_-\rangle \propto |n,j_+,j_- - 1\rangle. \tag{17}$$

Using these relations, the components in Eq. (14) obey the equations of motion

$$\frac{d}{dt}\langle J_x^+\rangle_{n,j_+,j_-} = \frac{i}{2}(E_{n,j_+,j_-} - E_{n,j_+-1,j_-})\langle \mathcal{J}_+^{\dagger}\rangle_{n,j_+,j_-} - \frac{i}{2}(E_{n,j_++1,j_-} - E_{n,j_+,j_-})\langle \mathcal{J}_+\rangle_{n,j_+,j_-},$$

$$\frac{d}{dt}\langle J_y^+\rangle_{n,j_+,j_-} = \frac{1}{2}(E_{n,j_+,j_-} - E_{n,j_+-1,j_-})\langle \mathcal{J}_+^{\dagger}\rangle_{n,j_+,j_-}$$

$$\frac{1}{2}(E_{n,j_++1,j_-} - E_{n,j_+,j_-})\langle \mathcal{J}_+\rangle_{n,j_+,j_-},$$

$$\frac{d}{dt}\langle J_z^+\rangle_{n,j_+,j_-} = 0. \tag{18}$$

By rewriting the energy difference as a derivative of the eigenenergy,

$$\omega_+ = -\frac{\partial H}{\partial J_z^+} \simeq E_{n,j_+,j_-} - E_{n,j_++1,j_-} = \frac{3}{2}nF \tag{19}$$

the equation becomes identical to the classical Bloch equation [Eq. (6)], i.e.,

$$\frac{d}{dt}\langle \vec{J}^+\rangle_{n,j_+,j_-} = \omega_+\langle \vec{J}^+\rangle_{n,j_+,j_-} \times \hat{z}. \tag{20}$$

The expectation values of the pseudospin operator, $\langle \vec{J}^+\rangle_{n,j_\pm,j_-}$, follow the dynamics of a single classical pseudospin $\langle \vec{J}^+\rangle_0$ (the same correspondence is obtained between $\langle \vec{J}^-\rangle_{n,j_+,j_-}$ and $\langle \vec{J}^-\rangle_0$). This is an obvious manifestation of the correspondence principle since the precessional motion is harmonic.

It is now of interest to identify the quantum analog to the classical adiabatic elimination of the fast time scale associated with the Kepler motion [see Eq. (5)]. This is implicit in Eq. (15) through the projection onto states of fixed n (and fixed energy E_n) which implies an average of the conjugate variable, i.e., time, over a duration $T_n \sim 2\pi(E_{n+1}-E_n)^{-1}$. For wave packets excited within a given n level, the average pseudospin follows the Bloch equation without damping [Eq. (20)], i.e.,

$$\frac{d}{dt}\langle \vec{J}^+\rangle_n = \omega_+\langle \vec{J}^+\rangle_n \times \hat{z} \tag{21}$$

with $\langle \vec{J}^+\rangle_n = \Sigma_{j_+,j_-}\langle \vec{J}^+\rangle_{n,j_+,j_-}$. For a wave packet with a superposition of neighboring n states over a narrow band Δn, the expectation value $\langle \vec{J}^+\rangle$ is given by the incoherent average over $\langle \vec{J}^+\rangle_n$,

$$\langle \vec{J}^+\rangle = \sum_n \langle \vec{J}^+\rangle_n. \tag{22}$$

This separability in the dynamics of the pseudospin component follows directly from the fact that the couplings between different n levels are eliminated through the operator replacement $[z \to -(3/2)n^2 A_z]$. At this level of approximation, the wave packet is reduced to an incoherent superposition of different n levels. Quantum beats on the time scale T_n are traced out.

For stronger fields, the coupling between different n levels, $\langle n,j_+,j_-|z|n',j_+',j_-'\rangle \neq 0$, becomes non-negligible. In the quadratic Stark regime the admixture from different n levels is taken into account in the eigenstates of the Stark Hamiltonian and the eigenenergies are given to second order in F by Eq. (10). The evolution of the pseudospins can still be approximated by the Bloch equation [Eq. (20)] although with the modified precession frequencies $\omega_\pm$ given by Eq. (12). The effects of n level mixing not accounted for by Eq. (20) give rise to dephasing, relaxation, or decoherence effects as they play now the role of environmental degrees of freedom.

III. PRECESSION AND DEPHASING

The accuracy of the classical [Eq. (6)] or quantum Bloch equation [Eq. (20)] in the limit of vanishing damping or relaxation can be tested by comparison with a full classical or quantum simulation. The latter includes the internal degrees of freedom traced out, i.e., the classical Kepler motion [Eq. (5)] or, equivalently, quantum mechanical inter-n coupling [Eq. (22)]. The neglected internal degree of freedom, electron motion along Kepler ellipses, is in this case interpreted as part of the environment. Damping due to this coupling is therefore included from the outset.

The dynamics of pseudospins are one dimensional in the reduced (or isolated) system. A single spin evolves through the azimuthal angle $\phi_\pm^J(t) = \omega_\pm t + \phi_\pm^J(0)$ with an angular velocity $\omega_\pm \simeq \pm(3/2)nF$ [Fig. 1(a)]. This behavior is illustrated for a single classical trajectory in Fig. 1(b) as a pseudospin initially oriented along the $-x$ axis in $n=350$ is subject to sudden application of a dc field ($F=20$ mV/cm) directed along the $+z$ axis. The time evolution resembles, to a good approximation, the precessional motion predicted by the first order Bloch equation. The Cartesian component J_x^+ undergoes nearly harmonic oscillations [Fig. 1(b)] for the time interval of observation (1 μs). We note that this result is obtained even without orbital period averaging [Eq. (5)] demonstrating that the fluctuations associated with the fast Kepler motion are indeed quite small.

This harmonic oscillation seen in the single-classical-pseudospin dynamics provides a vehicle to study classical-

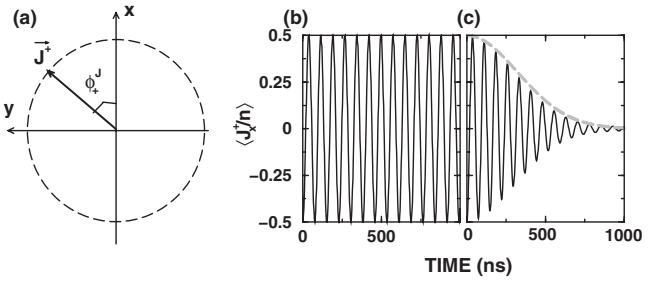

FIG. 1. (a) Schematic picture illustrating the precession of a pseudospin in the (J_x^+, J_y^+) plane. (b) Time evolution of J_x^+ for a single trajectory. (c) Ensemble average $\langle J_x^+ \rangle$ over 200 trajectories representing a 1D state. In (b) and (c), the initial state is oriented along the x axis with principal quantum number $n_i = 350$ and subject to sudden application (rise time ~300 ps) of a dc field $F = 20$ mV/cm. The gray dashed line corresponds to an average envelope function describing the relaxation, $0.5 \exp(-(\Gamma t)^2/2)$ with $\Gamma = 3.1$ rad/μs.

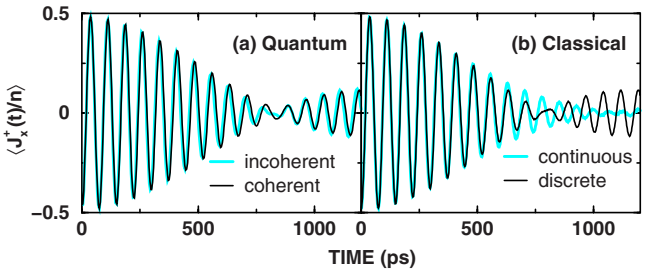

FIG. 2. (Color online) Calculated time evolutions of $\langle J_x^+ \rangle$ following sudden application (rise time ~300 fs) of a dc field of 200 V/cm. (a) Quantum wave packet: The initial state is either a coherent superposition of three ($n = 34$, 35, and 36) extreme redshifted parabolic states (oriented along the x axis) (black line) or an incoherent mixture of them [light blue (or gray) line, see Eqs. (13) and (26)]. (b) Classical wave packet: the initial state is a mix of restricted microcanonical ensembles with three discrete energies $E = -1/(2n^2)$ ($n = 34$, 35, or 36) (black line) or with a continuous energy distribution [Eq. (23)] with $\Delta n = 1$ [light blue (or gray) line]. Each of the restricted microcanonical ensembles corresponds to the extreme redshifted parabolic state.

quantum correspondence. For an ensemble of pseudospins, however, the situation can be different since quantum wave packets possess coherence between pseudospin components $\langle \vec{J}^+ \rangle_{n,j_+,j_-}$. We examine here if such coherence can play any role in the evolution of a wave packet, i.e., a pseudospin ensemble. We first consider the time evolution of an ensemble of classical pseudospins [see Fig. 1(c)] for which the effect of the ensemble average appears as "damping" of the harmonic oscillation. The pseudospins are initially oriented along the $-x$ axis (an ensemble of redshifted Stark states). The ensemble average $\langle J_x^\pm \rangle$ is calculated using the classical trajectory Monte Carlo (CTMC) method assuming an initial ensemble of phase space points given by

$$\rho_{\rm cl}^{\rm 1D}(\vec{r},\vec{p},0) = Cn^2 \exp\left(-\frac{(n-n_i)^2}{2(\Delta n)^2}\right)\chi_{-1}^1(L_x)\chi_{n-2}^n(nA_x), \tag{23}$$

where C is a normalization constant and χ_a^b is the characteristic function of the interval (a,b). The dependence on the phase space coordinates arises from n, L_x, and nA_x. These have initial mean values $\langle n \rangle = n_i = 350$ (as used experimentally), $\langle L_x \rangle = 0$, and $\langle nA_x \rangle = -n_i + 1$, representing extreme Stark states and yielding $\langle J_x^+ \rangle = -(n_i - 1)/2$, $\langle J_x^- \rangle = (n_i - 1)/2$. In the following, such an initial ensemble with $\Delta n = 13$ is termed for brevity the one-dimensional (1D) state. Because the ensemble Eq. (23) involves a finite Gaussian distribution of energy levels the oscillation amplitude of $\langle J_x^\pm(t) \rangle$ is clearly damped [see Fig. 1(c)]. The damping rate can be estimated using the spread in the precession frequencies, $\omega_+ \simeq (3/2)nF$, which depends only on n. Since n has a Gaussian distribution (assuming that the initial sudden application of F only slightly modifies the n distribution), the frequency spectrum will also have a Gaussian form with a width

$$\Delta\omega_+ = \frac{3}{2}\Delta nF \simeq 3.1 \text{ rad}/\mu\text{s}. \tag{24}$$

The damping envelope is thus also Gaussian, $\sim \exp[-(\Gamma t)^2/2]$, with a rate $\Gamma = \Delta\omega$ [see dashed line in Fig. 1(c)]. This strong damping results from the dephasing of the precessional motion [Fig. 1(a)], principally due to the frequency spread in the ensemble. This dephasing is given by the initial ensemble, is entirely deterministic, and is the atomic analog to the inhomogeneous line broadening in NMR. The inhomogeneity results in this case from the n distribution in the initial classical ensemble. As this process is deterministic rather than stochastic, this dephasing should be reversible, as will be analyzed in more detail below.

It is now instructive to compare the classical result with the time evolution of $\langle J_x^\pm \rangle$ for the corresponding quantum wave packet. We consider as an initial wave packet not only a pure state such as that in Eq. (13) but also an incoherent mixture of states to verify the separability of the dynamics among different n levels discussed in Eq. (22). As long as the approximation of relaxation-free Bloch equations holds (in the weak-field limit where inter-n couplings are negligible) a coherent initial state and an incoherent mixture should give identical results. Deviations result from weak couplings between different n levels, which are also responsible for decoherence. We calculate the time evolution of quantum wave packets (Fig. 2) by numerically solving the Schrödinger equation associated with the Hamiltonian [Eq. (2)]. Since quantum simulations for wave packets with $n_i \sim 350$ are demanding, we focus on a coherent superposition of extreme parabolic states around $n_i \sim 35$ oriented along the x axis,

$$|\psi(0)\rangle = \frac{1}{\sqrt{3}}\sum_{n=34}^{36}|\psi_n(0)\rangle, \tag{25}$$

where $|\psi_n(0)\rangle = |n, k_x = -n+1, m_x = 0\rangle$, and an incoherent ensemble encompassing the same states,

$$\rho_{\rm inc}(0) = \frac{1}{3}\sum_{n=34}^{36}|\psi_n(0)\rangle\langle\psi_n(0)|. \tag{26}$$

CTMC simulations for the same range of action ($n_i = 34-36$) have also been undertaken. By analogy to Eq. (26),

the initial state is chosen as an incoherent mix of microcanonical ensembles either with a continuous energy spectrum following Eq. (23) ($\Delta n=1$) or with three *discrete* (quantized) energies, i.e.,

$$\rho_{\rm cl}(\vec{r},\vec{p},0) = C \sum_{n_i=34}^{36} \delta\left(H_{\rm at} + \frac{1}{2n_i^2}\right) \chi_{-1}^{1}(L_x)\chi_{n-2}^{n}(nA_x) \quad (27)$$

where δ is a Dirac delta function.

When a dc field is applied transverse to the initial orientation of the pseudospins, the wave packet is no longer stationary. Each parabolic state $|n,k_x,m_x\rangle$ can be represented in the new basis, i.e., as a coherent superposition of parabolic states $|n,k,m\rangle$ defined along the z axis, i.e., parallel to the dc field. Since the dc field removes the degeneracy of those parabolic states $|n,k,m\rangle$, the pseudospins start precessing (Fig. 2). In view of the scaling relations, $F\propto n^{-4}$ and $t\propto n^3$, we employ a dc field of $F=200$ V/cm to mimic the dynamics that would be expected at $n=350$, assuming that classical scaling invariance holds. The pseudospin precesses and its amplitude is damped, but on a time scale of picoseconds instead of nanoseconds. As anticipated, the pseudospin precession and damping for the coherent and incoherent initial state are (nearly) identical in the presence of inhomogeneous line broadening. The observed damping can also be considered as transverse relaxation [3]. It does not involve any energy transfer to the system while thermal (longitudinal) relaxation would modify the occupation probability on each pseudospin component by transferring energy into the wave packet. Classical evolution predicted assuming a discrete energy spectrum [black line in Fig. 2(b)] and quantum dynamics [Fig. 2(a)] are in excellent agreement with each other for the time interval considered. The onset of a (fractional) "revival" at $t>900$ ns [Fig. 2(b)] is present not only in the quantum simulation but also in the classical simulation with discrete energies. On the other hand, the *conventional* classical simulation with a continuous energy spectrum exhibits damped oscillations without any revivals. Extrapolating this result to the very high Rydberg levels ($n_i\sim 350$) studied here, we can safely assume that the time evolution of $\langle\vec{J}^{\pm}\rangle$ is well predicted by CTMC calculations, i.e., the time scale of the dephasing of the pseudospin can be assumed to be short compared to the "quantum break time" $\tau_{\rm H}$ beyond which quantum observables deviate from their classical counterparts (when a continuous energy spectrum is assumed). For example, the observable $\langle\vec{J}^{\pm}\rangle$ shows a revival (the breakdown of classical-quantum correspondence) around 1 ns for $n=35$ and, consequently, 10 μs for $n=350$ since $\tau_{\rm H}\sim n^4$. For other observables, breakdown may occur somewhat earlier. Thus, in the following, all simulations for Rydberg wave packets with $n\sim 350$ are performed using the CTMC method. For the time interval considered (about ten precession periods in Fig. 1), damping due to inhomogeneous broadening dominates. This damping represents deterministic and thus reversible dephasing. This does not imply that irreversible dephasing or decoherence is absent. Since the simulation is based on the full classical Hamilton's equation of motion or the Schrödinger equation of the 3D Coulomb problem, inter-n couplings or temporal fluctuations due to the fast Kepler motion traced out in the Bloch-type equation is included. Accordingly, the damping rates include both homogeneous and inhomogeneous broadening. Separating the two is a challenge, in particular when their sizes are vastly different as in the present example. In the following we show that separating and extracting the rates becomes possible using echoes which can distinguish reversible dephasing (inhomogeneous dephasing) from irreversible dephasing (homogeneous dephasing).

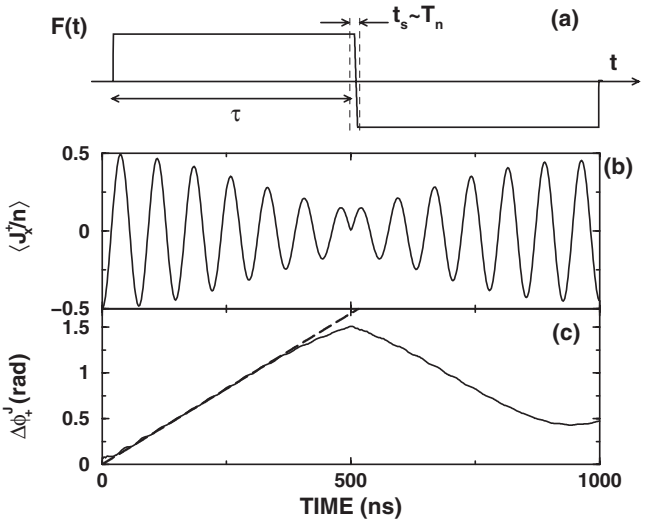

FIG. 3. (a) Electric field used to generate the echo in (b) and (c). Time evolution (b) of $\langle J_x^+(t)\rangle$ and (c) of the width of the azimuthal angle $\Delta\phi_{\pm}^J(t)$ predicted by CTMC simulations. The initial state is the $n_i=350$ 1D state and $\tau=500$ ns, $t_s=6.5$ ns, and $F=20$ mV/cm. The dashed line represents a linear growth in $\Delta\phi_+^J=\Gamma t$ with the damping rate $\Gamma=3.3$ rad/μs.

IV. ELECTRIC DIPOLE ECHOES

In order to separate reversible from irreversible dephasing we reverse the time axis by reversing the direction of pseudospin precession. This method is closely related to spin echoes in NMR [4]. Time reversal operates within the isolated system or within the "observed" degrees of freedom. For the unobserved degrees of freedom, such as the Kepler evolution, we cannot control the arrow of time. Consequently, this partial time reversal allows the discrimination of homogeneous and inhomogeneous broadening. In practice, it is not easy to reverse the arrow of time and generate rephasing. To examine the time reversibility of the pseudospin dynamics, it is necessary to perform an operation that (approximately) mimics time reversal within the reduced state space, i.e., reversal of the pseudospin precession. For electric dipoles, this can be accomplished in the linear Stark regime where the precession frequency $\omega_{\pm}\simeq\pm(3/2)nF$ is linear in F. Similar to the π pulse used to generate spin echoes in NMR [4], field reversal at $t=\tau$ [see Fig. 3(a)], i.e.,

$$F(t) = \begin{cases} F & \text{for } t < \tau - \frac{t_s}{2}, \\ F - \frac{2F}{t_s}\left(t - \tau + \frac{t_s}{2}\right) & \text{for } |t-\tau| < \frac{t_s}{2}, \\ -F & \text{for } t > \tau + \frac{t_s}{2} \end{cases} \quad (28)$$

reverses the direction of Stark precession, $\omega_\pm \to -\omega_\pm$. Here, t_s denotes the switching time, i.e., the finite time interval within which the field direction is reversed. The azimuthal angle $\phi^J_\pm(\tau) = \omega_\pm \tau + \phi^J_\pm(0)$ recovers its original value $\phi^J_\pm(2\tau) = -\omega_\pm \tau + \phi^J_\pm(\tau) = \phi^J_\pm(0)$ after another time interval τ. As seen in Figs. 1 and 2 an ensemble of pseudospins involving different actions n and thus different $\omega_\pm$ dephases and shows damping of the oscillations in $\langle J^\pm_x(t)\rangle$. By reversing the field direction at $\tau = 500$ ns, all pseudospins, independent of precession frequency, are time reversed and begin to rephase. As illustrated in Fig. 3(b), the initial amplitude is almost completely recovered after 2τ signaling an echo. Its strength can be quantified by the width of the distribution $\rho(\phi^J_\pm, t)$ in azimuthal angle $[\phi^J_\pm = \arctan(J^\pm_y / J^\pm_x)]$ defined as

$$\Delta\phi^J_\pm(t) = \{\langle[\delta\phi^J_\pm(t)]^2\rangle - \langle[\delta\phi^J_\pm(0)]^2\rangle\}^{1/2}, \quad (29)$$

where

$$\langle[\delta\phi^J_\pm(t)]^2\rangle = \int (\phi^J_\pm)^2 \rho(\phi^J_\pm, t) d\phi^J_\pm - \left(\int \phi^J_\pm \rho(\phi^J_\pm, t) d\phi^J_\pm\right)^2. \quad (30)$$

Zero spread $[\Delta\phi^J_\pm(2\tau) = 0]$ at the time of the echo, $t = 2\tau$, indicates full reversal and, therefore, a fully coherent ensemble. The difference between the fastest and the slowest frequencies determines the initial (linear) growth of the azimuthal width, $\Delta\phi^J_\pm(t) \propto (\omega^{\max}_\pm - \omega^{\min}_\pm)t$ [see Fig. 3(c)]. Thus, the initial slope $\Delta\phi^J_\pm(t)/t$ reflects the width of the frequency $(\omega_\pm)$ spectrum of the ensemble. Indeed, the slope in Fig. 3(c), 3.3 rad/μs, matches well the width of the frequency spectrum [Eq. (24)]. After field reversal, the broadened distribution is refocused. The minimum width $\Delta\phi^J_+ \simeq 0.4 \simeq 0.13\pi$ at $t \simeq 2\tau$ indicates a nearly perfect echo. We note that a small departure from linear behavior of $\Delta\phi^J_+$ becomes apparent before field reversal. This reflects the fact that the azimuthal angle is defined only within the range $[-\pi, \pi]$. Pseudospins can "accidentally" rephase when the azimuthal angles of different members of the ensemble are separated by an integer multiple of 2π.

A. Sources of irreversible dephasing

The residual imperfection in the rephasing at the echo time provides a direct quantitative measure of irreversible dephasing. For the current model system sources of decoherence are both intrinsic, i.e., atomic degrees of freedom not included in the pseudospin dynamics, and extrinsic, i.e., stochastic fluctuations in the experimental setup. We consider in the following first the intrinsic sources. The amplitude of the echoes is reduced in higher fields F when the high-order terms in $\omega_\pm$ become important. Due to the quadratic corrections, $\omega^{(2)}_k(F) = (3/8)n^4 kF^2$ and $\omega^{(2)}_m(F) = (9/8)n^4 mF^2$ [see Eq. (12)], the precession frequency is not precisely reversed by field reversal $(F \to -F)$ as is the case in the linear Stark regime. Quadratic corrections thus can provide an obstacle to time reversal. It turns out that the influence of the quadratic corrections can be controlled and suppressed. The echo seen in Fig. 3 for a relatively strong field is a case in point. In this case, the quadratic terms are suppressed because the initial extreme Stark states selected have $m = L_z \sim 0$ and $k = -nA_z \sim 0$ leading to a nearly perfect echo. Experimentally, preparing such an initial state in $n \simeq 350$ is quite a challenge. We therefore design alternative strategies to suppress such irreversible dephasing due to quadratic corrections in Sec. V.

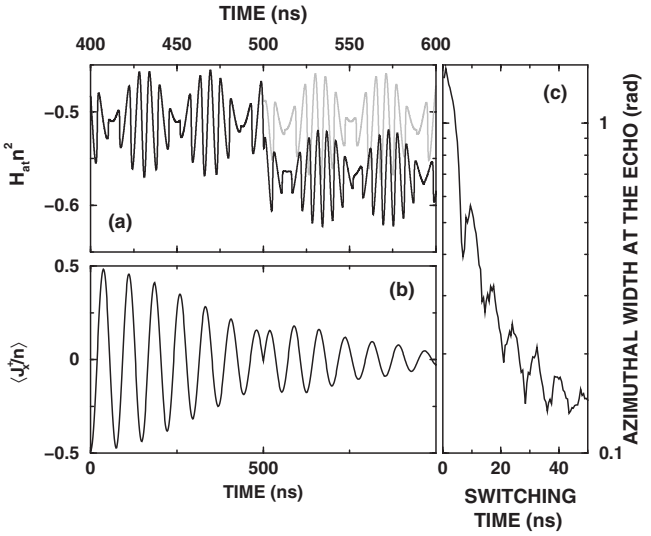

FIG. 4. (a) Time evolution of the unperturbed energy H_{at} for a single trajectory for two different switching times, $t_s = 0.5$ (black) and 6.5 ns (gray). (b) Time evolution of the ensemble average over trajectories $\langle J^+_x(t)\rangle$. The initial 1D state is subject to sudden application of a dc field ($F = 20$ mV/cm) and to a field reversal at $t = 500$ ns with $t_s = 0.5$ ns. (c) The minimum azimuthal width $\Delta\phi^J_+$ after field reversal (at the maximum echo) as a function of switching time t_s. The initial state and the applied field are the same as used in (b).

Nonadiabatic effects associated with switching on the field at time $t = 0$ as well as reversing it at time $t = \tau$ also contribute to irreversibility. One assumption made previously is that the action n, i.e., H_{at}, is time independent before and after the field reversal. However, H_{at} fluctuates in time. A typical evolution of $H_{at}(t)$ for a single trajectory is plotted in Fig. 4(a) and displays fast and slow oscillations associated with the Kepler orbital period (~6 ns) and about twice the frequency of the spin precession. The frequency doubling is due to the cylindrical symmetry of H_{at}. For a constant dc field, the total Hamiltonian H is time independent while $H_{at}(t) = H - Fz(t)$ oscillates in time through $z(t)$ with the Kepler period $T_n = 2\pi n^3 \simeq 6$ ns and the Stark period $[T_s = 2\pi/(3nF) \sim 40$ ns]. The nonadiabatic reversal (switching time $t_s = 500$ ps) of F at $t = \tau = 500$ ns induces transitions between different n levels and modifies the time average of the unperturbed energy H_{at} (dark solid line). The field reversal modifies the precession frequency $\omega_\pm \simeq \pm(3/2)nF$ not only in its sign but also in its magnitude, thereby breaking the

time-reversal symmetry. Consequently, the subsequent evolution of $J_x^+(t)$ displays a much smaller echo [Fig. 4(b)] than seen in Fig. 3(b). Unlike in other echo reversal operations (e.g., NMR), rapid nonadiabatic switching is detrimental to preserving time-reversal symmetry. The obvious reason is the presence of additional fast time scales (or nondegenerate energy levels) to which couplings become possible. Therefore, the switching time t_s should be chosen to be (at least) of the order of the orbital averaging time [Eq. (5)]. Indeed, with a nearly adiabatic field reversal (t_s=6.5 ns), the time-averaged Hamiltonian $H_{\rm at}$ is almost preserved during the field reversal [gray line in Fig. 4(a)] and approximate time reversal can be achieved. In fact, the forward-backward symmetry becomes even better when the switching time t_s is increased to the Stark period. The minimum azimuthal width $\Delta\phi_+^J$ after field reversal is plotted as a function of t_s in Fig. 4(c) and shows a clear decrease of $\Delta\phi_+^J$ with increasing switching time t_s. In particular, $\Delta\phi_+^J$ shows local minima at $t_s \simeq iT_n$ (i is an integer) because the energy $H_{\rm at}$ [Fig. 4(a)] (or position z) averaged over t_s becomes almost invariant for these switching times. Since in the Bloch equation [Eq. (6)] the Kepler evolution is a neglected degree of freedom, by choice of a suitable switching time the influence of the unobserved environmental degree of freedom and hence this source of decoherence can be controlled and minimized.

B. Determination of irreversible dephasing by multiple echoes

The initial growth in the azimuthal width $\Delta\phi_\pm^J$ is controlled by the spread of the frequency spectrum corresponding to the total dephasing rate associated with both reversible and irreversible dephasing. The irreversible dephasing can be viewed as the effect of stochastic fluctuations $\delta\omega_{\rm stoc}(t)$ in the precession frequency. Accordingly, the azimuthal angle at the time of the echo is

$$\phi_\pm^J(2\tau) = \phi_\pm^J(0) + \int_0^{2\tau} \delta\omega_{\rm stoc}(t)dt. \tag{31}$$

This stochastic coupling to the environment makes the azimuthal width grow at a higher rate. The echo technique described above allows the rate for irreversible dephasing to be extracted from the total rate. This method can be refined by exploiting multiple rather than single echoes. When a series of field reversals is applied at $t=\tau,3\tau,5\tau,\ldots$ [Fig. 5(a)], multiple echoes in the evolution of the pseudospins can be observed at $t=2\tau,4\tau,6\tau,\ldots$ [Fig. 5(b)]. The azimuthal angle distribution is refocused at each echo and its width shows a series of local minima [Fig. 5(c)]. Due to irreversible dephasing caused by quadratic Stark effects and nonadiabatic couplings during field reversal, the height of the local minima grows. The rate of irreversible dephasing can be extracted from the growth of these local minima in the azimuthal width $\Delta\phi_+^{\rm min}$ (thick dotted line). Assuming this growth is linear, the irreversible dephasing rate can be defined as the average slope,

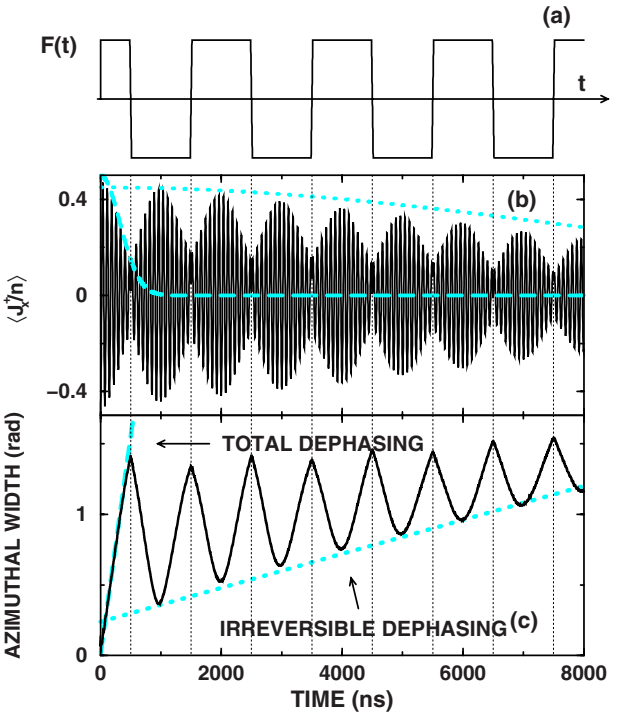

FIG. 5. (Color online) (a) Electric field sequence to observe multiple echoes. Field reversals are at $t=\tau,3\tau,5\tau,\ldots$. (In this plot τ=500 ns and t_s=6.5 ns.) (b) Time evolution of a pseudospin $J_x^+(t)$. The initial 1D state is subject to the time-dependent field depicted in (a) with extreme values of ±20 mV/cm. The thick dashed and dotted lines are proportional to $\exp[-(\Gamma t)^2/2]$ and $\exp[-(\Gamma_{\rm irr}t)^2/2]$, respectively. (c) Time evolution of the azimuthal width $\Delta\phi_+^J(t)$ for the same ensemble of wave packets as in (b). The thick dashed and dotted lines are proportional to Γt and $\Gamma_{\rm irr}t$, respectively. The dephasing rates are estimated from this plot as $\Gamma \simeq 3.1$ rad/μs and $\Gamma_{\rm irr} \simeq 0.12$ rad/μs. In (b) and (c), vertical dotted lines indicate the times of field reversals.

$$\Gamma_{\rm irr} = \left\langle \frac{\Delta\phi_+^{\rm min}(2(i+1)\tau) - \Delta\phi_+^{\rm min}(2i\tau)}{2\tau} \right\rangle. \tag{32}$$

In Fig. 5(c), a linear growth of the minima is observed for $t>1000$ ns yielding a dephasing rate $\Gamma_{\rm irr}$=0.12 rad/μs. This is to be compared with the total rate, Γ=3.1 rad/μs [thick dashed line in Fig. 5(b)], with which the amplitude of the beats of the pseudospin $J_x^+(t)$ initially dephases.

The Fourier transform of $\langle J_x^+(t)\rangle$ manifests these two dephasing rates even more clearly. Without field reversal [see an example of $\langle J_x^+(t)\rangle$ in Fig. 1(c)] the Fourier transform, as shown in Fig. 6(a), is approximately Gaussian with a width associated with the total dephasing rate, i.e., $\Delta\nu=\Gamma/(2\pi) \simeq 0.5$ MHz, around the precession frequency $\omega_\pm/(2\pi) \simeq 13.5$ MHz. In contrast, the Fourier transforms of $\langle J_x^+(t)\rangle$ when a series of field reversals is applied exhibit a set of discrete peaks separated by the frequency of the multiple echo sequence, $1/(2\tau) \sim 1$ MHz [Figs. 6(b) and 6(c)]. Each peak has a width corresponding to the irreversible dephasing rate $\Delta\nu_{\rm irr}=\Gamma_{\rm irr}/(2\pi) \simeq 20$ kHz and the relative height of each peak follows the Gaussian envelope (dashed line) associated with the total rate. For a characteristic reversal time τ

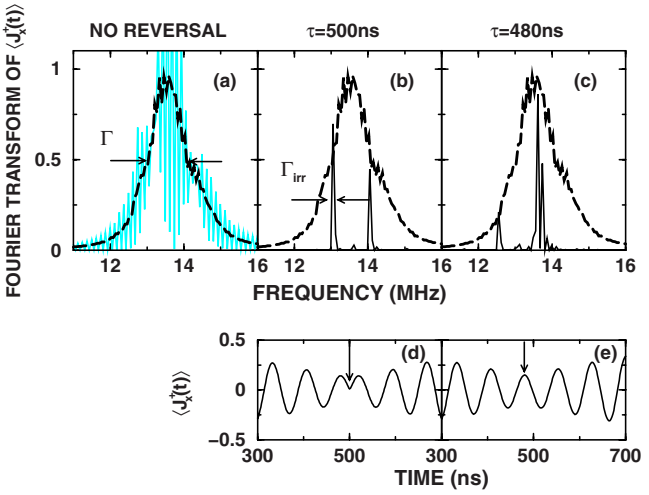

FIG. 6. (Color online) Fourier transforms of $\langle J_x^+(t)\rangle$. The initial 1D state is subject to a dc field ($F=20$ mV/cm) (a) without field reversal and with a series of field reversals at $\tau=$(b) 500 and (c) 480 ns (see text). The raw Fourier spectrum shown by the colored (gray) line in (a) exhibits strong fluctuations but the smoothed distribution (black dashed line) follows a Gaussian distribution. This smoothed spectrum is also plotted in (b) and (c). Each frame is normalized to the same peak heights to better compare the envelope shapes. The lower panels show the time evolution of $\langle J_x^+(t)\rangle$ near a field reversal at $\tau=$(d) 500 and (e) 480 ns. The time of field reversal is indicated by an arrow.

=500 ns, the phase of the pseudospin oscillations [see Fig. 6(d)] is shifted by π at field reversals leading to the disappearance of the main peak at the precession frequency (13.5 MHz) in the Fourier spectrum. A small shift of the reversal time to $\tau=480$ ns [Fig. 6(e)] prevents this phase shift and the contribution near the precession frequency is recovered.

The irreversible dephasing rates obtained by multiple echoes are well defined and nearly independent of the reversal time τ. Figure 7(a) shows the evolution of the azimuthal width for three different reversal times, $\tau=100,200,500$ ns.

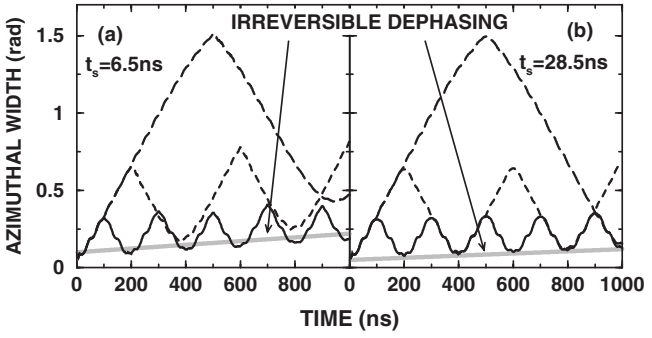

FIG. 7. Calculated time evolution of the azimuthal width $\Delta\phi_+^J(t)$. The initial 1D state is subject to a dc field ($F=20$ mV/cm) with a series of field reversals with characteristic times $\tau=100$ (solid line), 200 (dashed line), and $\tau=500$ (long-dashed line). The switching times t_s are (a) 6.5 ($\sim T_n$) and (b) 28.5 ns ($\gg T_n$). Gray lines indicate the growth due to irreversible dephasing.

The minimum azimuthal width at each echo grows linearly at a rate $\Gamma_{\rm irr}\simeq 0.12$ rad/μs in agreement with the estimate derived from the azimuthal width in Fig. 5(c). This irreversible rate can be reduced by choosing a larger switching time t_s (Fig. 4). A switching time of $t_s=28.5$ ns is found to be optimal for suppression of irreversible dephasing. In this optimal case, $\Gamma_{\rm irr}$ is reduced to $\Gamma_{\rm irr}\simeq 0.07$ rad/μs [Fig. 7(b)].

C. Relation to revivals

Revivals of quantum beats [16,17] are a well-studied signature of the persistence of coherence in the time evolution of quantum wave packets. While the quantum beats, in the present case Stark beats, may have a classical analog, their revivals generally do not because they rely on the discreteness of the excitation spectrum. (For the comparison in Fig. 2, we introduced such discrete excitation energies into the classical simulation through choice of the initial states in order to disentangle the quantum effect due to discreteness from that due to phase coherence.) Revivals are observed for systems with discrete and nonequispaced eigenenergy spectra. Only when a finite number of frequency components contribute to the time evolution of an observable, will a dephased ensemble rephase (with a phase shift of an integer multiple of 2π) within a finite time and exhibit quantum beat revivals. Stark wave packets for relatively low n levels are a good example as they possess only a few frequency components in their spectra. The onset of (fractional) revivals seen for $n\simeq 35$ in Fig. 2(a) with a frequency spectrum consisting of three discrete components $\omega_+=(3/2)nF$ with $n=34$, 35, and 36 is one such example. The key point is that the amplitude of these revivals is reduced by decoherence which reduces the discreteness of the frequency spectrum. Thus, the size of the revivals provides an alternative measure of decoherence. There are, however, important differences between revivals and echoes. One difference is that the revival time $\tau_{\rm R}$ is given by the discrete frequency spectrum and cannot be controlled. For high-lying Rydberg states, the density of discrete frequencies becomes high. More specifically, for Rydberg wavepackets with $n=350$, there are about 20–30 frequency components within the Gaussian envelope depicted in Fig. 6(a). Correspondingly, the revival time is expected to be more than 10 μs. Even if coherence could be, in principle, preserved, such long time intervals are not accessible in the current experiment. More generally, $\tau_{\rm R}$ is of the order of the Heisenberg time $\tau_{\rm H}\sim n^4$ and thus difficult to realize in high Rydberg states. Therefore, determination of irreversible dephasing via revivals becomes impossible. In contrast, the echo time can be controlled and made sufficiently short that irreversible dephasing becomes accessible on short time scales ($\leqslant 1$ μs) even though the dephasing time to be measured ($\Gamma_{\rm irr}^{-1}$) may be much longer ($\Gamma_{\rm irr}^{-1}\gtrsim 10$ μs). Echoes are thus a versatile tool to measure decoherence and dephasing on a time scale much shorter than can be achieved using revivals.

V. CONTROLLING DEPHASING

We consider now protocols that allow the control and manipulation of dephasing in Rydberg atoms. Irreversible

dephasing can be reduced by effectively eliminating contributions due to the quadratic Stark effect or can be enhanced by exposing Rydberg atoms to external synthesized noise whose spectral content can be controlled.

A. Suppression of irreversible dephasing due to the quadratic Stark effect

Experimentally, it is not easy to prepare a wave packet like the 1D state assumed in the above discussions. While it is feasible to produce oriented wave packets [18,19], they are usually less oriented than the 1D state. Because a finite range of k and m values are excited, quadratic Stark effects play an important role in determining the size of echoes. They can be effectively suppressed, however, by monitoring the echo in observables that are cylindrically symmetric about the z axis. To illustrate this, we transform the equation of motion into a rotating frame

$$\vec{K}^{\pm} = R_z(\phi = \omega_m^{(2)} t)\vec{J}^{\pm}, \tag{33}$$

where $R_z(\phi)$ is the rotation matrix by an angle ϕ about the z axis. Since, to leading order, the quadratic Stark effect modifies only the precession frequency in the Bloch equations [Eq. (6)], the equation in the rotating frame becomes

$$\frac{d}{dt}\vec{K}^{\pm} = \pm\, \omega_k(F)\vec{K}^{\pm} \times \hat{z}. \tag{34}$$

The two pseudospins in the rotating frame, $\vec{K}^{\pm}$, precess in opposite directions but at identical rates $\omega_k(F) = \omega_k^{(1)}(F) - \omega_k^{(2)}(F)$. The precession of $\vec{J}^{\pm}$ with frequency $\omega_m^{(2)}(F)$ in the laboratory frame is thus removed.

We analyze now the effect of the term $\omega_k^{(2)} \sim F^2$ in ω_k by examining the time evolution of an experimentally accessible wave packet in the rotating frame using CTMC simulations. The wave packet is initially a mix of redshifted Stark states characterized by the actions $n=350$, $L_x=0$, having nA_x randomly distributed according to a Gaussian distribution centered at $\bar{k}_x=299$ with spread $\Delta k_x=20$. [We call this initial state a quasi-one-dimensional (quasi-1D) state.] The wave packet is initially oriented along the x axis. Figure 8(a) displays the behavior of $\langle J_x^+(t)\rangle$ (in the laboratory frame). While the initial state consists of only a single n level, sudden application of the dc field (rise time ~300 ps) induces transitions between different n levels, in particular for trajectories misaligned relative to the x axis. This broadens the distribution of precession frequencies and, consequently, the oscillation amplitude of the pseudospin is reduced. For inhomogeneous broadening due to the nonadiabatic field switch-on, the n distribution, and, in turn, the frequency distribution, is better approximated by an exponential rather than a Gaussian function. Sudden application of the dc field transfers an energy $\Delta E \simeq zF$ to the electron and the n distribution reflects the initial distribution projected on the z axis which is closer to exponential. Thus, the damping of the pseudospin oscillations follows a Lorentzian envelope $\sim 1/[1+(\Gamma t)^2/2]$. After field reversal, the damping due to inhomogeneous broadening continues. The absence of an echo results from the presence of the $\sim\omega_m^{(2)}(F)$ contribution due to the quadratic Stark effect. A mirror image of $\langle J_x^+(t)\rangle$ $(0<t<500$ ns) is included in the figure (in light blue or gray) to highlight the differences between the predicted continued damping and the time-reversed $\langle J_x^+(t)\rangle$. Switching now to observables in the rotating frame [Eq. (33)], dephasing is markedly different: the pseudospin $\langle K_x^+(t)\rangle$ in the rotating frame shows a very clear echo. We can examine the size of the echo using the azimuthal width $\Delta\phi_+$ for the three different alignments ($k_x = 299, 249, 199$) of the initial state [Fig. 8(c)] [$\phi_\pm = \arctan(K_y^\pm/K_x^\pm)$ is the azimuthal angle in the rotating frame while $\phi_\pm^J$ is the azimuthal angle in the laboratory frame]. The minimum widths after field reversal range from $\Delta\phi_+ = 0.4$ to 0.5 rad, which is slightly larger than that seen in Fig. 3(c). Upon removing the m dependent part, $\omega_m^{(2)}$, of the quadratic correction, a strong echo is recovered. Note, however, that the m-independent part $\omega_k^{(2)}$ is still present. The latter is reduced by the initial alignment along the x axis. Even when the orientation of the initial state is changed substantially, the azimuthal width at the time of the echo is little modified [Fig. 8(c)]. Thus, by using oriented wave packets and applying a transverse dc field, the quadratic correction $\omega_k^{(2)}(F)$ does not dramatically affect the observation of echoes.

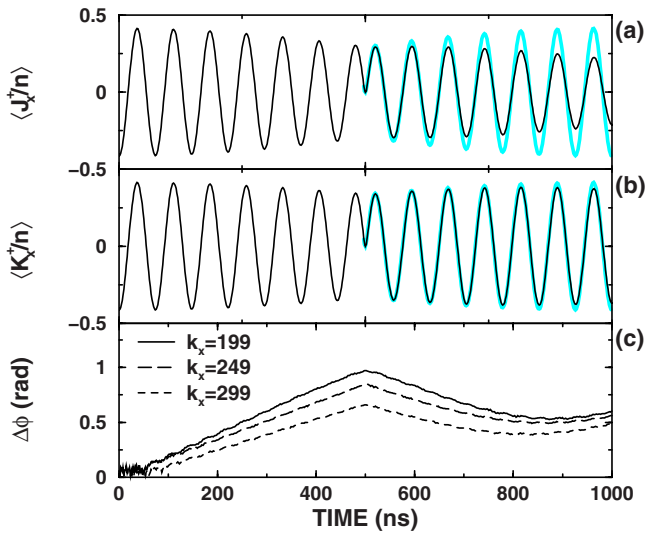

FIG. 8. (Color online) Calculated evolution of the pseudospins in (a) the laboratory frame and (b) the rotating frame, and (c) of the azimuthal width in the rotating frame. The initial state is a mix of Stark states oriented along the x axis ($n=350$, $L_x=0$, $nA_x \in [-\bar{k}_x-2\Delta k_x, -\bar{k}_x+2\Delta k_x]$ with $\Delta k_x=20$.) In (a) and (b), the average action is set to $\bar{k}_x=299$ and in (c) three different values $\bar{k}_x = 199, 249, 299$ are chosen. For comparison, a mirror image of the first half $(0<t<500$ ns) of $J_x^+(t)$ and $K_x^+(t)$ is shown by the light blue (gray) thick line in (a) and (b).

Experimentally, one cannot switch to the rotating frame directly but one can instead focus on observables that are cylindrically symmetric about the z axis (the dc field axis). They exhibit Stark echoes without being dephased by the quadratic contribution $\omega_m^{(2)}(F)$ since those variables are invariant under transformation from the laboratory to the rotating frame. The electron coordinate $\langle z(t)\rangle$ and momentum $\langle p_z(t)\rangle$ are candidates for such variables. We choose in the following as observable the survival probability $P_s(t_{\text{delay}})$ fol-

lowing application of a probe half-cycle pulse (HCP) directed along the z axis at a variable time delay $t=t_{\rm delay}$ measured from the time $t=0$ when the sudden dc field is applied. $P_s(t_{\rm delay})$ is closely related to $\langle p_z\rangle$ and can be easily measured experimentally. When the duration of the probe HCP is much shorter than the electron orbital period, $T_n=2\pi n^3$ ($\sim$6.5 ns for $n=350$), the HCP simply delivers an impulsive momentum transfer or "kick," $\Delta p=-\int F_{\rm HCP}(t)dt$, to the excited electron. Ionization is determined by the energy gain $\Delta E(p_z)=p_z\Delta p+(\Delta p)^2/2$ which is a function of the momentum p_z at the time of the application of the HCP. The survival probability thus mirrors the evolution of $\langle p_z(t)\rangle$ of the wave packet. The time evolution of the elongation and orientation of the Kepler ellipse due to the Stark precession results in a time-dependent survival probability. The survival probability for a single classical trajectory oscillates with both the Kepler and the precession frequency. Thus, the time-dependent survival probability has (approximately) the same frequency spectrum as that of pseudospin precession. The survival probability can therefore be used to extract the total as well as the irreversible dephasing rates. We note again (see the discussion of Fig. 4) that for cylindrically symmetric observables the frequency is doubled with $\omega_s=(\omega_+-\omega_-)\simeq 3nF$ being the Stark frequency corresponding to the energy splitting between adjacent Stark states. The absolute azimuthal angles of each pseudospin $\vec{J}^{\pm}$ are not probed separately, only their relative angle which evolves with the doubled frequency as $\phi_+-\phi_-\sim\omega_+t-\omega_-t=2\omega_+t$.

The calculated survival probability for the quasi-1D initial state [Fig. 9(a)] displays fast oscillations (period $\sim$6 ns) associated with the Kepler orbit and slower variations (period $\sim$40 ns) associated with the relative pseudospin precession. Similarly to $J_x^+(t)$ [Fig. 1(c)], the oscillation amplitude is damped due to dephasing. Without field reversal the damping continues [black line in Fig. 9(b)] while a clear echo is observed following field reversal at $t=500$ ns [gray line in Fig. 9(b)]. In this simulation the direction of the probe pulse is also reversed following field reversal, so that symmetry is preserved before and after the field reversal, leading to an accurate time reversal. In order to relate $P_s(t_{\rm delay})$ to the Bloch equation [Eq. (6)] we average the survival probability over the fast Kepler motion with a period T_n [Figs. 9(c) and 9(d)]. As a result of this coarse graining [Eq. (5)], only the beating associated with pseudospin precession is seen. With doubling of the oscillation frequency relative to that seen in Fig. 8(b) comes also the doubling of the relaxation rate. The dephasing rates are twice as large as those ($\Gamma=1.36$ rad/μs and $\Gamma_{\rm irr}=0.36$ rad/μs) derived from Fig. 8(c).

B. External noise

In order to extend the dynamical range of relaxation rates to be probed, we manipulate the irreversible dephasing rate by applying external noise. "External" refers here to the external fields rather than to atomic degrees traced out.

The effect of colored noise on the total dephasing of Stark beats has been studied in a controlled manner using artificially synthesized noise [20]. The noise used is generated as a randomly alternating binary-valued electric field

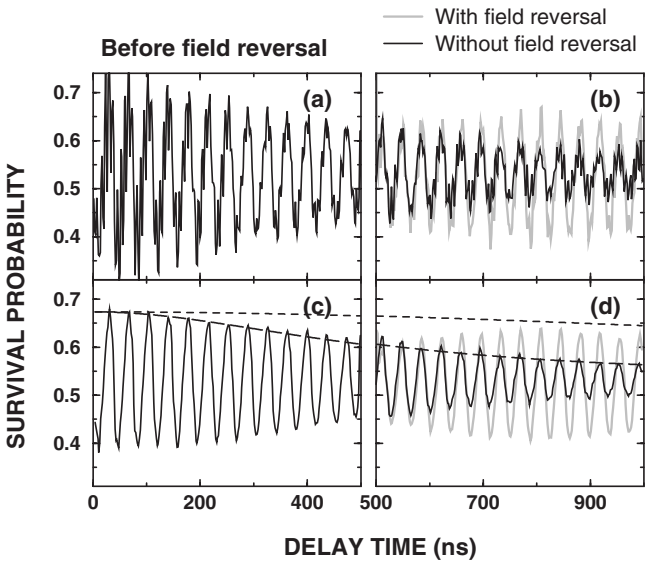

FIG. 9. Calculated survival probability as a function of delay time $t_{\rm delay}$. The initial quasi-1D state ($n=350$) is subject to sudden application (rise time $\sim$300 ps) of a dc field with $F=20$ mV/cm with a superposed probe HCP ($\Delta p_{\rm probe}=-0.532n$) at $t=t_{\rm delay}$. Early [$t<500$ ns (a)] and late [$t>500$ ns (b)] times are shown in separate frames. The gray line in (b) indicates the probability for $t>500$ ns when a field reversal is applied at $t=500$ ns with $t_s=6.5$ ns. The orientation of the probe pulse is also reversed ($\Delta p_{\rm probe}=+0.532n$). (c) and (d) probabilities obtained by averaging those in (a) and (b) over a Kepler period $T_n=6.5$ ns. The oscillation amplitude and the size of the echo are damped as $\sim 1/[1+2(\Gamma t)^2]$ (dashed line) and $\sim 1/[1+2(\Gamma_{\rm irr}t)^2]$ (dotted line), respectively. The dephasing rates are obtained from Fig. 8 as $\Gamma=1.36$ rad/μs and $\Gamma_{\rm irr}=0.36$ rad/μs.

$$F_{\rm ran}(t)=\sum_{j\geq 1}F_j\chi^{jT_{\rm ran}}_{(j-1)T_{\rm ran}}(t) \tag{35}$$

where

$$F_j=\pm\Delta F \tag{36}$$

and $\chi^{jT_{\rm ran}}_{(j-1)T_{\rm ran}}(t)$ is the characteristic function of the interval $[(j-1)T_{\rm ran},jT_{\rm ran}]$. $F_{\rm ran}(t)$ discontinuously jumps randomly between these two values of F_j after fixed time intervals $T_{\rm ran}$ and remains constant $F_{\rm ran}(t)=F_j$ during each interval $(j-1)T_{\rm ran}<t<jT_{\rm ran}$. We define the characteristic frequency of this noise as $\nu_c=1/(2T_{\rm ran})=\nu_{\rm ran}/2$ corresponding to the frequency for an alternating sequence $\Delta F,-\Delta F,\Delta F,\ldots$. The average frequency obtained using the power spectrum of $F_{\rm ran}(t)$ is in fact smaller than ν_c (see [20] for details). This random noise is superposed on the static field. Single or multiple reversal(s) of this field are considered and the ensemble average taken over different random noise sequences for each trajectory is calculated to quantify the rate of irreversible dephasing.

Figure 10 displays the evolution of the azimuthal width of the initial quasi-1D state subject to a static field having multiple reversals with characteristic time $\tau=200$ ns when, in addition, noise with amplitude $\Delta F=0.1F$ and $\nu_c=1/T_n=150$ MHz or $1/(2T_n)=75$ MHz is applied. Assuming first

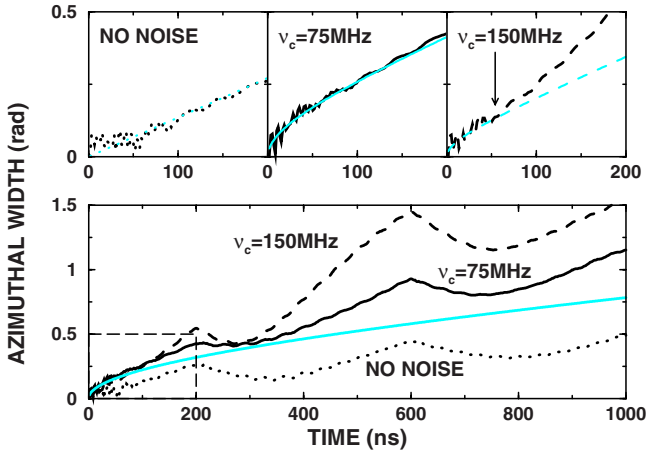

FIG. 10. (Color online) Calculated evolution of the azimuthal width $\Delta\phi_+(t)$ for the initial quasi-1D state when subject to a static field with multiple reversals at $t=200$ and 600 ns (dotted line), and when noise $F_{\rm ran}(t)$ is superposed with $\nu_c=75$ MHz (solid line), and with $\nu_c=150$ MHz (dashed line). The upper panels show blowups of the time interval $0<t<200$ ns (indicated by the dashed square). The light blue (gray) lines correspond to the analytical predictions [Eq. (38)] with $\Gamma(\Delta F=0)=1.36$ rad/μs for the upper panels and [Eq. (40)] with $\Gamma(\Delta F=0)=3.6$ rad/μs for the lower panel (only predictions for $\nu_c=75$ MHz are included.)

for simplicity that noise would leave the initial n distribution created by the nonadiabatic switch-on invariant, the time evolution of the azimuthal angle for a single trajectory in the presence of noise is given to order $\sim\Delta F$ by

$$\phi_+(t)=\omega_+(\Delta F=0)t+\frac{3}{2}n\langle F_{\rm ran}\rangle_t t+O(\Delta F^2), \qquad (37)$$

where $\langle F_{\rm ran}\rangle_t=t^{-1}\int_0^t F_{\rm ran}(t')dt'$. The azimuthal width in the presence of noise is increased to

$$\Delta\phi_+(t)=t\sqrt{\Gamma(\Delta F=0)^2+\frac{9}{4}n^2\sum_{\eta=1}^{N_\eta}\langle F_{\rm ran}^\eta\rangle_t^2}, \qquad (38)$$

where the average is taken over stochastic realizations of the random field ($\eta=1,2,\ldots,N_\eta$). The time-average random field $\langle F_{\rm ran}\rangle_t$ vanishes in the limit $t\to\infty$. For short periods the square deviation $\Sigma_{\eta=1}^{N_\eta}\langle F_{\rm ran}^\eta\rangle_t^2$ decays inversely with time as $\Sigma_{\eta=1}^{N_\eta}\langle F_{\rm ran}^\eta\rangle_t^2=(\Delta F)^2T_{\rm ran}/t$. Using the noise-free dephasing rate $\Gamma(\Delta F=0)=1.36$ rad/μs (derived from Fig. 8) we can estimate the initial growth in azimuthal width using Eq. (38) (this is illustrated by the upper panels in Fig. 10).

One limitation of Eq. (38) is the assumption that the spread in n is unaffected by the noise. The latter assumption depends critically on the color, i.e., the frequency distribution, of the noise. By tuning the artificially synthesized noise spectrum relative to the excitation spectrum of the high Rydberg states, the excitation dynamics can be significantly influenced. Briefly, when the characteristic frequency ν_c of the noise satisfies the resonance condition $\nu_c^{-1}=jT_n$ (j is an odd integer), the noise and the Kepler motion of the electron constructively interfere, leading to excitation of the electron (a change in n) modifying, in turn, the precession frequency $\omega_s\simeq 3nF$. Consequently, the wave packet shows enhanced dephasing. On the other hand, for an even integer j in the resonance condition, the electronic motion destructively interferes with the noise, leading to little change in n and little additional dephasing. At late times, the transitions between different n levels induced by the noise becomes significant and the evolution of the azimuthal angle is modified to

$$\phi_+(t)\simeq\omega_+(\Delta F=0)t+\frac{3}{2}n\langle F_{\rm ran}\rangle_t t+\frac{3}{2}(\Delta n)Ft \qquad (39)$$

where Δn denotes noise-induced broadening of the n distribution. For $\nu_c=150$ MHz, the constructive interferences between Kepler motion $z(t)$ and the random field $F_{\rm ran}(t)$ induces transitions and further accelerates dephasing as can be already observed at early times ($t\simeq 50$ ns, denoted by an arrow in Fig. 10). It can be seen more clearly in the irreversible dephasing rate extracted from the local minima in $\Delta\phi_+$ at the time of echoes at $t\simeq 400$, and 800 ns. The irreversible dephasing rate is increased by the nonvanishing time-average field $\langle F_{\rm ran}\rangle_t$ (similar to the total dephasing rate [Eq. (38)]) as

$$\Delta\phi_+(t)=t\sqrt{\Gamma_{\rm irr}(\Delta F=0)^2+\frac{9}{4}n^2\sum_{\eta=1}^{N_\eta}\langle F_{\rm ran}^\eta\rangle_t^2}. \qquad (40)$$

For $\nu_c=75$ MHz, this estimate reproduces the irreversible rate indicating that the broadening Δn is suppressed for an extended period. On the other hand, irreversible dephasing is faster for $\nu_c=1/T_n=150$ MHz. Thus, by tuning the characteristic noise frequency to induce Δn transitions, the reversibility of the dynamics can be effectively destroyed.

VI. EXPERIMENTAL REALIZATION

The apparatus used to investigate Stark echoes experimentally is described in detail elsewhere [19,21]. Briefly, quasi-one-dimensional Rydberg atoms oriented along the x axis are first produced by photoexciting potassium atoms to a mix of the lowest-lying redshifted states in the $n=350$ Stark manifold in a weak ($\sim$250 μV cm^{-1}) dc field (directed along the x axis) [21]. A much larger dc field $F=20$ mV cm^{-1} is then suddenly applied (rise time ~ 0.3 ns$\ll T_n$) in the z direction [Fig. 3(a)] to create a Stark wave packet comprising a coherent superposition of Stark states with a narrow range of n. The wave packet is subject to a single field reversal or to multiple field reversals at $t=\tau,3\tau,\ldots$ with a switching time of $t_s\sim 7$ ns$\sim T_n$. The echo is monitored by applying a probe HCP of duration $T_p\sim 0.6$ ns and amplitude sufficient to ionize $\sim$50% of the atoms, along the z axis after a variable time delay $\tau_{\rm delay}$ and measuring the overall survival probability (after the dc field has returned to zero) using field ionization [8]. The total duration of the dc field is limited to ~ 1 μs by the output characteristics of the pulse generators used to establish the field.

A. Single-reversal measurement

Figure 11(a) shows the measured survival probability following a single field reversal as a function of time delay $\tau_{\rm delay}$ between the application of the dc field and the probe

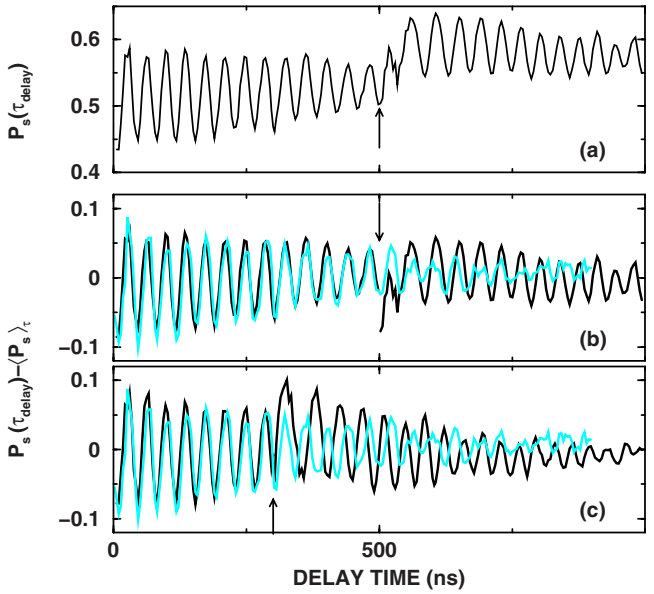

FIG. 11. (Color online) (a) Measured survival probability for the quasi-1D initial state subject to sudden application of a dc field (F=20 mV/cm and rise time of 300 ps) with field reversal at τ =500 ns (switching time t_s=7 ns). A probe HCP with scaled momentum transfer Δp_0=−0.532 and pulse duration of 600 ps is applied at a variable delay time. (b) Measured probabilities in (a) are split into two parts, $t<500$ ns and $t>500$ ns and for each part the oscillations in survival probability are shifted such that their average is zero. (c) Measured probability as in (b) but the field is reversed at t=300 ns. The arrows indicate the times of the field reversal. The light blue (gray) lines in (b) and (c) show the survival probabilities observed without field reversal. All data are smoothed over an orbital period, ~7 ns.

pulse. An echo similar to that seen in Figs. 9(c) and 9(d) is clearly observed. Some differences are apparent, however, such as the reduced amplitude of the beats and the small shift in the time-averaged survival probability before and after field reversal. The former is accounted for by uncertainties of the distribution of quasi-1D states initially prepared. The results in Fig. 9 were derived using a mix of the redshifted states in the Stark manifold centered around $k\sim 299$ and having an average scaled dipole moment $\langle d_0\rangle\sim -1.3$. This distribution is based on calculated oscillator strengths for excitation from the ground state. The actual mix of states excited in the experiment, however, depends on the effective laser linewidth (~12 MHz) governed mostly by the laser and atom beam divergences and by the exact laser tuning. Furthermore, even though stray fields in the experimental region can be reduced to $<50\ \mu\mathrm{V\ cm^{-1}}$ [21], their presence still leads to uncertainties in the magnitude and direction of the applied Stark field. These effects will reduce the average dipole moment and the amplitude of the oscillations in the survival probability.

A small increase in the average survival probability at the point of field reversal is observed when the probe pulse is applied after field reversal. This is because the pulse when applied before field reversal leads to production of a range of higher-n states that do not behave adiabatically when the field is reversed and can be ionized by field reversal. To preserve the symmetry relative to the point of field reversal, in the calculations the orientation of the probe pulse was reversed when applied after the field reversal (Fig. 9). Experimentally, it is, in principle, possible to follow a similar protocol by performing two separate measurements: one without field reversal for $\tau_{\mathrm{delay}}<500$ ns and one with a field reversal for $\tau_{\mathrm{delay}}<500$ ns. In such a protocol, however, it is difficult to maintain coherence between the two measurements since a slight change of the dc field strength or the probe kick strength will induce additional decoherence. One more practical way to eliminate the shift in the survival probability is to split the data into two parts, before and after the field reversal, and subtract the time-averaged probability from each of them [Fig. 11(b)]. The small shift of the average survival probability is removed and the amplitude of the oscillations before and after field reversal can be directly compared. Due to the reduced dipole of the initial state, the echo is less obvious than in Fig. 9. However, when compared with the survival probability without field reversal, it is clear that the wave packets are rephased and the survival probability shows a recovery of the oscillation amplitude. By examining the size of echoes as a function of field reversal time it is possible to extract the rate of irreversible dephasing [22].

B. Measurements with multiple reversals

Data obtained for multiple field reversals at $t=\tau,3\tau,5\tau,\ldots$ are shown in Fig. 12 for τ=100 and 200 ns. As in the case of single reversal, the survival probability is split into several segments for adjacent field reversals, i.e., $0<t<\tau$, $\tau<t<3\tau$, $3\tau<t<5\tau,\cdots$. In each segment, the average probability is subtracted such that the variations in the echo amplitude can be directly compared. For τ=100 and 200 ns, a Lorentzian envelope is fitted to the decay of the echoes and the irreversible dephasing rate estimated as Γ_{irr}=0.6 rad/μs. This is slightly larger than that extracted from the CTMC simulation in Fig. 9 (0.36 rad/μs) and can be attributed partly to contributions associated with additional "noise" existing in the experimental setup not accounted for in the simulations and partly to the uncertainty of the average dipole of the initial state. The latter has, indirectly, an influence on the irreversible dephasing rate: the smaller the average dipole is, the less aligned is the initial state. In turn, the k-dependent part of the second-order Stark contributions of the precession frequency, $\omega_k^{(2)}$, become larger and induce stronger irreversible dephasing (see Sec. V). Nevertheless, extraction of atomic irreversible dephasing times on a multimicrosecond time scale is possible and the results agree with simulations to within a factor 2.

C. Noise-induced dephasing

Noise-induced irreversible dephasing can be enhanced by adding artificially synthesized noise. This allows study of the stochastic interactions with the environment in a controlled manner. The noise is produced by superposing the output from a (gated) random pulse generator on the dc field while maintaining the time-averaged dc field experienced by the atoms unchanged. The generator divides time into a series of bins of adjustable width and in each randomly assigns an

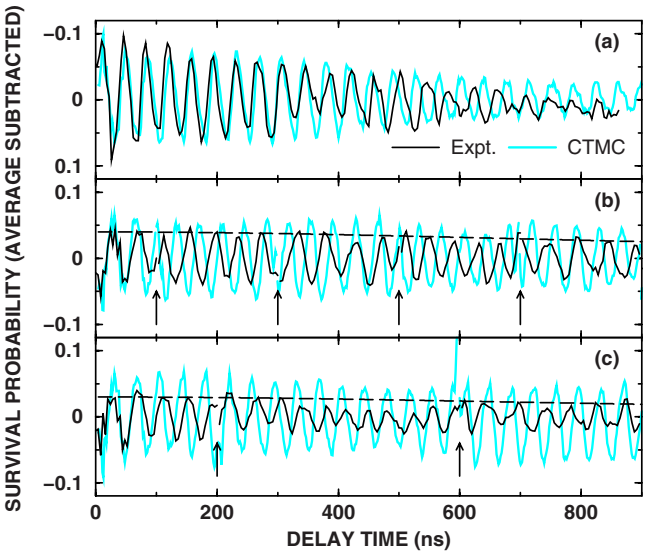

FIG. 12. (Color online) Measured (black) and calculated (light blue or gray) survival probabilities after subtraction of the average values (see text) for the quasi-1D initial state subject to sudden application of a dc field ($F=20$ mV/cm and rise time of 300 ps) (a) without field reversal and with multiple reversals for $\tau=$(b) 100, and (c) 200 ns. The damping of the oscillation amplitude has an envelope with a Lorentzian form $\sim 1/[1+2(\Gamma_{\rm irr}t)^2]$ with $\Gamma_{\rm irr}=0.6$ rad/μs [dashed lines in (b) and (c)]. The arrows indicate the times of field reversals. The probe HCP (pulse duration $\sim$600 ps) has a scaled momentum transfer $\Delta p_0=-0.53$ in (a) and -0.46 in (b) and (c). All data are smoothed over an orbital period $\sim$7 ns. The calculations assume a mixture of initial quasi-1D states with an average dipole moment $\langle d\rangle=-0.75$.

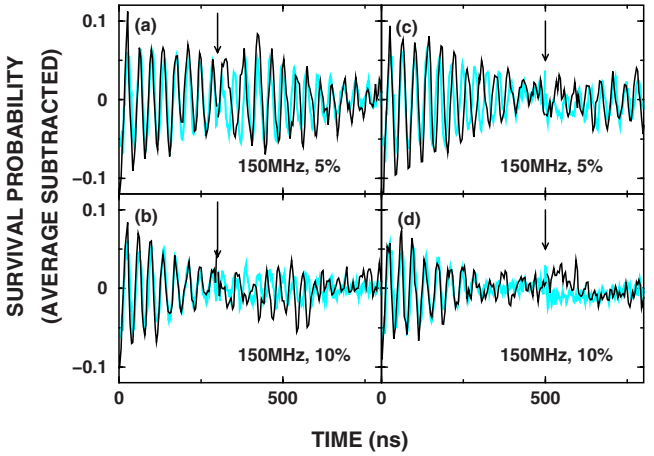

FIG. 13. (Color online) Measured (black) and calculated (light blue or gray) survival probabilities for the quasi-1D initial state ($\langle d\rangle=-0.75$) subject to sudden application of a dc field ($F=20$ mV/cm and rise time of 300 ps) with a field reversal at $\tau=300$ (a), (b) or 500 ns (c), (d) (indicated by arrows) and switching time $t_s=7$ ns in the presence of noise with amplitude $\Delta F/F=\pm 0.05$ (a), (c) or ± 0.1 (b), (d) and characteristic frequency $\nu_c=150$ MHz. The probe HCP used has a scaled momentum transfer $\Delta p_0=-0.46$. All data are smoothed over an orbital period $\sim$7 ns.

output of 0 or V. V is chosen such that the peak-to-peak amplitude of the noise is $\sim$5–10 % that of the time-averaged dc field. The survival probabilities shown in Fig. 13 were averaged over many cycles each using a different random sequence of noise. The characteristic frequency of the noise was $\nu_c=150$ MHz. Compared to Figs. 11(a) or 12(a), the initial damping of the oscillations is much more rapid indicating that both reversible and irreversible dephasing is enhanced by the fluctuating field. Since the noise frequency is resonant with the Kepler orbital frequency, the induced transitions between different n levels are expected to accelerate irreversible dephasing. For small noise amplitudes [$\Delta F/F=5\%$ in Figs. 13(a) and 13(c)] the wave packet remains at least partly coherent for extended periods and echoes can be observed at $t\sim 500$ ns in Fig. 13(a) and $\sim$800 ns in Fig. 13(c). For 10% noise amplitude, irreversible dephasing is much more rapid. While small echoes can be still seen but at $t\sim 500$ ns in Fig. 13(b), almost no trace of echoes is observed at $t\sim 800$ ns. In all cases, the agreement between measurements and simulations is remarkable.

VII. CONCLUSIONS AND OUTLOOK

We have demonstrated that by reversing the applied field the pseudospins associated with Rydberg Stark wave packets can be rephased to generate quantum beat echoes. Multiple reversals lead to a series of echoes whose amplitudes decrease with time. From their decay rate, the irreversible dephasing rate can be determined. The irreversible dephasing rate can be increased by the presence of noise and is sensitive to its characteristic frequency spectrum. When the noise frequency resonantly matches the energy difference between neighboring n levels, the irreversible dephasing rate is enhanced not only due to the fluctuations in the dc field magnitude but also due to transitions to adjacent levels that modify the pseudospin precession frequencies.

In the present protocol, time reversal is achieved by reversing the direction of the external dc field. However, this operation reverses the arrow of time only for certain degrees of freedom, the precession of pseudospins. The resulting echo can thus be used as a measure for coherence of the dynamics of pseudospins with other atomic degrees of freedom treated as environmental degrees of freedom. When the pseudospins are coupled to neglected degrees of freedom, those which are not time reversed by a field reversal, the size of the echo is reduced. This can be identified as intra-atomic irreversible dephasing. The dephasing times due to intra-atomic couplings estimated classically are comparable to the quantum break time. It would therefore be interesting to investigate any quantum effects on the dephasing time by treating the intra-atomic couplings quantum mechanically. It is, however, experimentally challenging to measure small changes in dephasing times on the order of microseconds.

The coherence of pseudospins, or equivalently, of electric dipole moments of Rydberg atoms may be of interest for the study of ultracold Rydberg atoms. The average (coarse-grained) electric dipole moment of an atom affects the eigenenergy spectrum of other neighboring atoms resulting in phenomena such as the dipole-dipole blockade [23]. Information concerning coherent dynamics in such a strongly correlated system might be extracted by examining the dynam-

ics in the "reduced" Hilbert space. The echo technique can be used to probe the interaction strength between atoms through deviations from the behavior expected for isolated atoms. In such a setting, the present treatment of intra-atomic decoherence should be extended to interatomic decoherence involving the relevant degrees of freedom of the dipole-coupled atomic pair.

Our present protocol for generating dipole echoes in Rydberg atoms bears considerable resemblance to that used to generate a spin echo [4]. One significant difference is that for the latter time reversal is achieved by reversing the orientations of spins relative to the applied magnetic field, which is kept constant. This reversal is very likely to preserve the inhomogeneity of the magnetic field and thus the inhomogeneous broadening is reversible. In the case of Stark echoes, however, the time reversal is implemented by modulating the dc field and, consequently, the inhomogeneity in the field may not be perfectly preserved before and after field reversals. Thus, the broadening, conventionally considered to be "inhomogeneous," may contribute to irreversible dephasing. Similar to a spin echo, a π pulse (an alternating field perpendicular to the dc field) could be used to flip the orientations of pseudospins to achieve time reversal. However, for the Stark precession, such time reversal is quite challenging since two pseudospins $\vec{J}^{+}$ and $\vec{J}^{-}$ precessing in opposite directions have to be manipulated simultaneously to observe echoes. The observation of echoes in the current protocol proves that external sources for decoherence are reasonably well under control in the present experimental apparatus. Only with the application of relatively strong additional noise does the dynamics become completely irreversible destroying the echo.

ACKNOWLEDGMENTS

S.Y. and J.B. acknowledge support by the FWF-SFB016 (Austria). C.O.R. acknowledges support by the OBES and U.S. DOE to ORNL, which is managed by the UT-Batelle LLC under Contract No. DE-4C05-00OR22725. Research at Rice is supported by the NSF under Grant No. PHY-0650732 and by the Robert A. Welch Foundation under Grant No. C-0734.

[1] W. H. Zurek, Rev. Mod. Phys. **75**, 715 (2003); N. Gisin, G. Ribordy, W. Tittel, and H. Zbinden, *ibid.* **74**, 145 (2002); A. Barenco, D. Deutsch, A. Ekert, and R. Jozsa, Phys. Rev. Lett. **74**, 4083 (1995); P. W. Shor, Phys. Rev. A **52**, R2493 (1995).
[2] M. D. Lukin, Rev. Mod. Phys. **75**, 457 (2003).
[3] C. P. Slichter, *Principles of Magnetic Resonance* (Springer, New York, 1992).
[4] E. L. Hahn, Phys. Rev. **80**, 580 (1950).
[5] I. D. Abella, N. A. Kurnit, and S. R. Hartmann, Phys. Rev. **141**, 391 (1966).
[6] T. H. Jeys, F. B. Dunning, and R. F. Stebbings, Phys. Rev. A **29**, 379 (1984).
[7] R. S. Minns, M. R. Kutteruf, H. Zaidi, L. Ko, and R. R. Jones, Phys. Rev. Lett. **97**, 040504 (2006).
[8] S. Yoshida, C. O. Reinhold, J. Burgdörfer, W. Zhao, J. J. Mestayer, J. C. Lancaster, and F. B. Dunning, Phys. Rev. Lett. **98**, 203004 (2007).
[9] L. D. Landau and E. M. Lifshitz, *Mechanics* (Pergamon Press, Oxford, 1960).
[10] I. C. Percival and D. Richards, J. Phys. B **12**, 2051 (1979).
[11] T. P. Hezel, C. E. Burkhardt, M. Ciocca, and J. J. Leventhal, Am. J. Phys. **60**, 324 (1992).
[12] A. J. Lichtenberg and M. A. Lieberman, *Regular and Chaotic Dynamics*, 2nd ed., Applied Mathematical Sciences Vol. 38 (Spriner-Verlag, New York, 1992).
[13] F. Bloch, Phys. Rev. **70**, 460 (1946).
[14] P. Bellomo and C. R. Stroud, Jr., Phys. Rev. A **59**, 2139 (1999).
[15] W. Pauli, Z. Phys. **36**, 336 (1926).
[16] R. Bluhm, V. A. Kostelecky, and B. Tudose, Phys. Rev. A **55**, 819 (1997).
[17] H. Wen, S. N. Pisharody, J. M. Murray, and P. H. Bucksbaum, Phys. Rev. A **71**, 013407 (2005).
[18] A. ten Wolde, L. D. Noordam, A. Lagendijk, and H. B. van Linden van den Heuvell, Phys. Rev. A **40**, 485 (1989).
[19] C. L. Stokely, J. C. Lancaster, F. B. Dunning, D. G. Arbó, C. O. Reinhold, and J. Burgdörfer, Phys. Rev. A **67**, 013403 (2003).
[20] S. Yoshida, C. O. Reinhold, J. Burgdörfer, W. Zhao, J. J. Mestayer, J. C. Lancaster, and F. B. Dunning, Phys. Rev. A **75**, 013414 (2007).
[21] F. B. Dunning, J. C. Lancaster, C. O. Reinhold, S. Yoshida, and J. Burgdörfer, Adv. At., Mol., Opt. Phys. **52**, 49 (2005).
[22] H. Y. Carr and E. M. Purcell, Phys. Rev. **94**, 630 (1954).
[23] M. D. Lukin, M. Fleischhauer, R. Cote, L. M. Duan, D. Jaksch, J. I. Cirac, and P. Zoller, Phys. Rev. Lett. **87**, 037901 (2001).